RAPID COMMUNICATION

Ultrasonic preparation of mesoporous silica using pyridinium ionic liquid

Ana-Maria Putz*, Adél Len**, Catalin Ianăşi*, Cecilia Savii*, and László Almásy**,†

*Institute of Chemistry Timisoara of Romanian Academy, Laboratory of Inorganic Chemistry,
Bv. MihaiViteazul, No. 24, RO-300223 Timisoara, Romania
**Wigner Research Centre for Physics, Institute for Solid State Physics and Optics, POB 49 Budapest-1525, Hungary

Abstract−Mesoporous silica matrices have been prepared via classic acid catalyzed and sono-catalyzed sol-gel routes. Tetramethoxysilan (TMOS) and methyl-trimethoxysilane (MTMS) were used as silica precursors, and N-butyl-3-methylpyridinium tetrafluoroborate ([bmPy][BF$_4$]) was employed as co-solvent and pore template. The ionic liquid (IL) to silica mole ratio was varied between 0.007 and 0.07. Nitrogen adsorption-desorption and small-angle neutron scattering measurements were used to characterize the obtained materials. The ionic liquid played the role of catalyst that affected the formation of the primary xerogel particles, and changed the porosity of the materials. Ultrasound treatment resulted in microstructure change on the level of the colloid particle aggregates. In comparison with IL containing xerogels, the IL containing sonogels show increased pore diameter, bigger pore volumes and diminished surface areas.

Keywords: Ionic Liquid, Ultrasound, SANS, TMOS (Tetramethoxysilane), MTMS (Trimethoxymethylsilane)

INTRODUCTION

Ionic liquids (ILs) are salts that are liquid below 100 °C and consist of a large organic cation together with an organic or inorganic anion [1,2]. ILs can be used as reaction medium for inorganic materials due to their intrinsic high charge density and polarizability [3,4]. ILs pre-organized structure makes them suitable as templates for the porous materials [3,4]. ILs used as templating agent can increase the thermal stability of the synthesized materials [5]. As solvents in the sol-gel process, ILs negligible vapor pressure prevents evaporation and their high ionic strength increases the speed of aggregation [6]. Shrinkage and syneresis are reduced during gelation and aging; therefore, due to a limited collapse of the pores during solvent extraction, highly porous silica matrixes can be synthesized [7,8]. Besides their role as co-solvents, ILs also show catalytic activity. The pyridinium groups of the cations behave as Brønsted acidic catalysts that accelerate the hydrolysis of silica precursors, while the tetrafluoroborate anion behaves as Lewis base catalysts that accelerate the condensation reactions of silica [9].

Use of methylated precursors leads to water stable and time stable ionogels [10,11] and improves immobilization of substituted porphyrins [12]. Besides inducing hydrophobicity, the bulky IL cations also help to control the pore size [5]. It was shown that [bmPy][BF$_4$] or [bmIm][BF$_4$] (at molar ratio IL/Si=1.6 and IL/Si=0.07, respectively) causes a significant increase in the average pore radius, in comparison with similar materials prepared without IL [4].

Sonication is an alternative method to stimulate the hydrolysis

of the alkoxide without using alcoholic solvents in the sol-gel process [13,14]. Strong ultrasound action (20-100 kHz) induces chemical reactions and/or enhances their rate [15]. Soft sonication augments the aging of the starting solutions [16,17].

In the present study, nanostructured xerogels and sono-activated gels were prepared by using N-butyl-3-methylpyridinium tetrafluoroborate [bmPy][BF$_4$] ionic liquid (IL) as co-solvent, at IL/Si molar ratios from 0.007 : 1 to 0.07 : 1. Tetramethoxysilan (TMOS) and methyltrimethoxysilane (MTMS) were used as precursors; TMOS was chosen because it leads to faster hydrolysis in comparison with TEOS [18]. The obtained materials were characterized by FT-IR spectroscopy, nitrogen adsorption and small-angle neutron scattering.

EXPERIMENTAL

1. Synthesis Conditions

All reagents were used as received: N-butyl-3-methylpyridinium tetrafluoroborate ([bmPy][BF$_4$], for synthesis 98%, Merck); the silicon precursors: methyl-trimethoxysilane (MTMS, 98%, Merck) and tetramethoxysilane (TMOS, 98%, Merck); distilled water; and hydrochloric acid (HCl, 37%, S.C. SilalTreding SRL). MTMS to TMOS molar proportion of 1 : 8 was used for all samples.

Two series of samples, classic xerogels and sonicated gels, were prepared using a modified recipe of Karout and Pierre [4]. The synthesis started by mixing 0.13 moles TMOS, 1.15 moles distilled water, 0.4 moles acidic water (adjusted to pH=2.8 by addition of HCl) and 0.01615 moles MTMS.

In the case of xerogel series, the reaction mixture was mechanically vigorously stirred for 15 minutes in a round bottom flask until a homogeneous sol was obtained. At this point, for each sample, aqueous [bmPy][BF$_4$] solution was added into the reaction mixture in various IL/Si molar ratios, within 0.007 to 0.07 range, (see Table 1) under continuous stirring for 15 minutes. The obtained

†To whom correspondence should be addressed.
E-mail: almasy@mail.kfki.hu

Table 1. Synthesis parameters

Xerogel samples	Sonogel samples	Molar ratio IL/Si	IL [g]	TMOS [g]	MTMS [g]
0X	0S	0	0	19.8	2.2
1X	1S	0.007	0.25	19.8	2.2
2X	2S	0.018	0.62	19.8	2.2
3X	3S	0.034	1.19	19.8	2.2
4X	4S	0.053	1.85	19.8	2.2
5X	5S	0.07	2.46	19.8	2.2

sols were left to gel, in covered vessels, at room temperature. The xerogel samples labelled as 0X-60, 1X-60, 2X-60, 3X-60, 4X-60 and 5X-60 were obtained by drying the silica gel at 60 °C for 26 h (Table 1). For 0X-60, instead of the aqueous ionic liquid solution, an equal volume of distilled water was added.

A second series of samples, 0S-60, 1S-60, 2S-60, 3S-60, 4S-60 and 5S-60, was synthesized by using the same recipe, but instead of mechanical stirring, ultrasonication was applied starting from adding of the first reactant into the reaction mixture, till the end.

A VCX-T - 750 apparatus operating at 20 kHz and 750 W, with titanium sonotrode (1 cm diameter) was immersed (1 cm deep) into the sol. The sonotrode worked at 25% amplitude, with pulse sequence on/off - 15/5 sec. A 150 mL sample container was filled with 95 mL of liquid for each preparation. During sonication (23 minutes) the temperature increased from 25 °C to 60 °C. The total transferred energy, including thermal dissipation, was 250 J/mL for each sample.

2. Thermal Treatment

The 0X-60, 5X-60 and 5S-60 samples were thermally successively treated, in air, at 150 °C for 90 minutes (labelled 0X-150, 5X-150, 5S-150); at 500 °C for 60 minutes (labelled 0X-500, 5X-500, 5S-500); and at 1,000 °C for 60 minutes, labelled as 0X-1000, 5X-1000 and 5S-1000.

3. Materials Characterisation

FT-IR spectra of the powders in KBr pellets were registered on a JASCO-FT/IR-4200 apparatus. Textural properties of the composite silica matrix samples were analyzed using nitrogen adsorption/desorption measurements at liquid nitrogen temperature (77 K) with a Quantachrome Nova 1200e instrument. Prior to the measurements the samples were degassed during three hours at 100 °C, in flow nitrogen atmosphere. The specific surface area (S_{BET}) was calculated from the Brunauer, Emmett and Teller (BET) equation, the total pore volume (V_p) was determined from the last point of adsorption and the pore diameter (D_p) determined by Barrett, Joyner and Halenda (BJH) method, from the adsorption and desorption branches of the isotherms, using a NovaWin software. The pore size distribution (PSD) was calculated by the DFT method.

The small angle neutron scattering (SANS) measurements were performed at the *Yellow Submarine* spectrometer at the Budapest Neutron Centre [19]. Samples were measured at ambient temperature.

RESULTS AND DISCUSSION

1. Gelation Time

As IL content was increasing, the gelation time was decreasing,

specifically, from 24 h to 5 h for the xerogel series and from 126 h to instant gelation for the sonogel series; therefore, the catalytic role of IL was evidenced.

2. FT-IR Analysis

The broad band between 3,474-3,441 cm^{-1} corresponds to the overlapping of the O-H stretching bands of hydrogen-bonded water molecules (H-O-H…H) and SiO-H stretching of surface silanols hydrogen-bonded to molecular water (SiO-H…H$_2$O) [20,21]. This band is more intense in the sample synthesized without IL, in both xerogels (Fig. 1) and the calcined samples (Fig. 2), indicating that IL's presence strengthens the hydrophobic character. The adsorbed water deformation vibration bands [21,22] appear at 1,635 cm^{-1} as well.

The intense and broad band which appears at 1,099-1,075 cm^{-1} is assigned to the transversal optical (TO) modes of the Si-O-Si asymmetric stretching vibrations [21,23]. The presence of the sila-
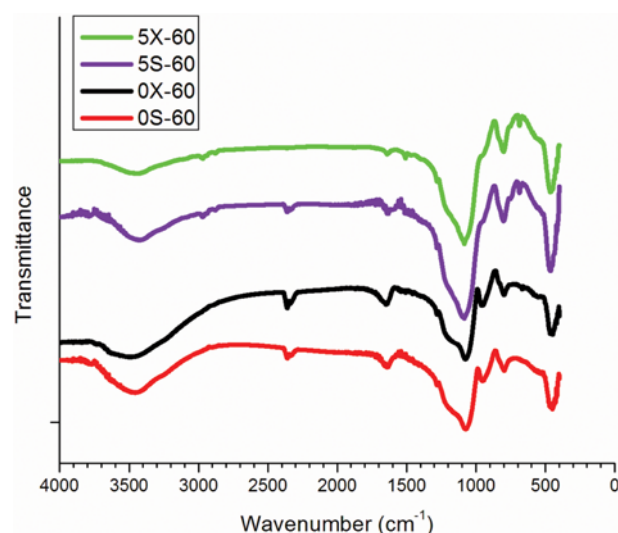

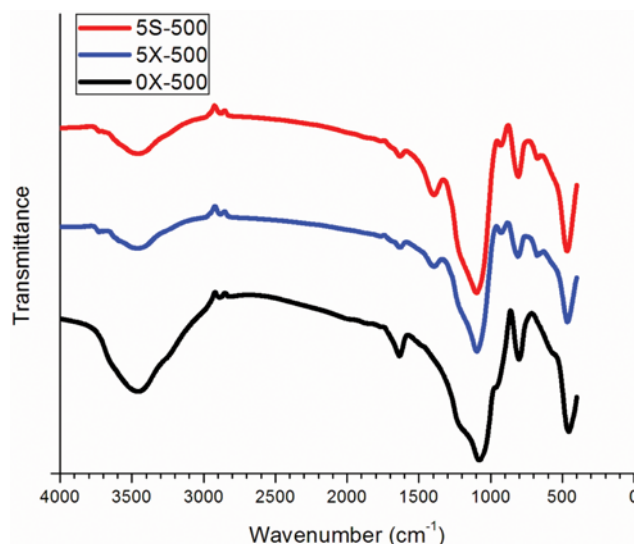**Fig. 1. IR spectra of the xerogels 0X-60, 1X-60, 5X-60, and sonogels 0S-60, 1S-60, 5S-60.**

Fig. 2. IR spectra of the calcined samples 0X-500, 5X-500 and 5S-500.

Table 2. Textural properties of the xerogels and sonogels

Sample	Surface area BET [m²/g]	Pore diameter [nm] Ads	Pore diameter [nm] Des	Total pore volume [cm³/g]
0X-60	774.8	3.62	3.64	0.424
1X-60	535.7	3.62	3.63	0.452
2X-60	446.9	3.61	3.67	0.552
3X-60	389.8	4.62	3.65	0.542
4X-60	308.2	6.18	4.56	0.509
5X-60	248.0	4.62	4.69	0.397
0S-60	943.7	3.61	3.61	0.709
1S-60	542.6	3.39	3.86	0.523
2S-60	373.0	5.58	4.34	0.554
3S-60	390.2	5.58	4.93	0.592
4S-60	172.1	7.67	6.61	0.362
5S-60	214.0	9.04	7.87	0.682

nol groups was confirmed by the band centered about $960\,cm^{-1}$, which is associated with the stretching mode of the Si-OH groups [24]. The symmetric stretching vibrations of Si-O-Si appear at $800\,cm^{-1}$ and $680\,cm^{-1}$ [20,21,25] and its bending mode appears at $467\text{-}458\,cm^{-1}$ [21,24,26,27].

The band from $2{,}970\text{-}2{,}975\,cm^{-1}$ corresponds to the asymmetric C-H stretching vibration of methyl group from the IL [28] and its disappearance after calcinations at $500\,^{\circ}C$ shows that the bmPy cation is largely removed.

Adsorption bands of the IL were not observed in our samples. The characteristic $1{,}027\,cm^{-1}$ band of pure [bmPy][BF$_4$] overlapped with the broad band of the silica matrix at $1{,}084\,cm^{-1}$ and could not be distinguished [29]; The Si-O-Si asymmetric stretching vibrations were shifted to slightly higher wave numbers with the increase of calcinations temperature, while the symmetric stretching vibrations and their bending mode were shifted to slightly lower wave numbers. With the increase of the calcinations temperature (from 150 to $500\,^{\circ}C$), the bands assigned to antisymmetric deformation bending of CH$_2$ groups [shifted from $1{,}509\,cm^{-1}$ (60C and 150C IL samples), to $1{,}396\,cm^{-1}$ (for 500C IL samples]. These changes indicate a restructuring of the silica network following the elimination of the ionic liquid and the pore collapse (shown by nitrogen adsorp-

tion). The 1640 and 960 bands characteristic of the Si-OH become weaker, indicating water loss. The IR data did not show visible differences between xerogels and sonogels (see Figs. 1 and 2).

3. Nitrogen Adsorption-desorption Isotherms

It is well known that increased surface tension causes pore collapsing; therefore, the reduction of the surface tension by the IL content is favorable for porosity preservation [4]. As a general observation, within both the xerogels and the sonogels series, the pore size was continuously increasing with increasing IL concentration (Table 2). At small IL content (1X-60 and 2X-60 samples) the values of the pore diameters from adsorption are close to those calculated from desorption, which indicates more regular pore shapes in these samples. In xerogel and sonogel synthesized without IL regular pore shapes are obtained as well.

The mean pore size, calculated from the desorption branch of isotherms using BJH method, increases from 3.64 nm (0X-60 sample) to 4.68 nm (5X-60 sample) and from 3.61 nm (0S-60 sample) to 7.87 nm (5S-60 sample) for the sonogels (Table 3). Similar trends are obtained from the adsorption branches and by DFT method (see Table 2). The pore size in sonogel (5S-60 sample) is almost double compared to the corresponding xerogel (5X-60 sample).

The specific surface area is decreasing with the increase of IL

Table 3. Textural properties of the thermally treated samples

Sample	Surface area BET [m²/g]	Pore diameter [nm] Ads.	Pore diameter [nm] Des.	Pore diameter [nm] DFT	Total pore volume [cm³/g]
5X-60	248.0	4.238	4.682	5.880	0.397
5x-150	215.7	6.218	4.682	6.079	0.371
5x-500	94.91	15.191	8.955	18.55	0.448
5x-700	71.93	15.716	17.82	17.91	0.329
5x-1000	57.34	3.717	17.57	3.418	0.165
5s-60	214.0	15.287	9.038	9.773	0.682
5s-150	188.5	15.150	8.959	9.773	0.647
5s-500	103.3	4.278	16.27	3.418	0.425
5s-700	61.51	3.726	25.24	27.37	0.218
5s-1000	63.34	3.656	3.58	3.934	0.118

Fig. 3. Nitrogen adsorption/desorption isotherms of the xerogel and sonogel samples.

Fig. 4. Nitrogen adsorption/desorption isotherms of the xerogel and sonogel samples calcined at different temperatures.

concentration, in both, xerogels and sonogels, after a sharp step-like decrease between the 0X-60 and 1X-60, (and 0X-60 and 1S-60) samples.

With the increase of calcination temperature, the specific surface area continuously decreases in both series until 700 °C. The pore diameter increased in both xerogels and sonogels as IL was removed. The surface area reduction during calcination was stronger for the xerogel series compared to sonogel series, indicating that sonogels were more resistant to calcination.

3-1. Nitrogen Adsorption-desorption Isotherms for Xerogels and Sonogels Dried at 60 °C

Nitrogen adsorption isotherms of samples dried at 60 °C are shown in Fig. 3. The xerogel sample without IL, 0X-60, has Type IV isotherms with H4 hysteresis loop which is often associated with narrow slit-like pore [30]. The xerogel samples synthesized with IL, have Type IV isotherm with H2 characteristic hysteresis loops attributable to the materials with ink-bottle pore shapes [31]. The pore diameters from adsorption reflect the size of the bottle, and the pore diameters from desorption can be associated with the necks between pores [32]. The sonogel sample synthesized without IL, 0S-60, and the sonogels samples with IL content up to 0.053 mole fraction present Type IV isotherm with H2 characteristic hysteresis loops. The sonogel sample with the highest concentration of IL, 5S-60, has Type IV isotherm with H1 characteristic hysteresis loops, associated with porous materials which exhibit a narrow distribution of relatively uniform pores [31].

3-2. Nitrogen Adsorption-desorption Isotherms for the Thermally Treated Samples

Isotherms of the thermally treated samples are shown in Fig. 4. For the xerogel series, sample 5X-150 has Type IV isotherm with H2 hysteresis loop. By heating at 500 °C, 700 °C and 1,000 °C, it changes to Type IV isotherms with H3 hysteresis loops, characteristic of slit shaped pores [33]. These data suggest that in order to obtain uniform pores the calcination temperatures should be below 500 °C.

In the case of sonogels, Type IV isotherm with H1 hysteresis loops was obtained both for the sample dried at 60 °C, as well as after thermal treatment at 150 °C. Further calcination at 500 °C
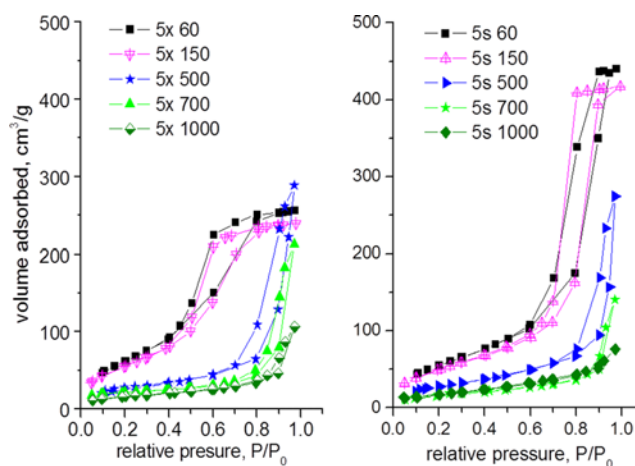
and 700 °C leads to Type IV isotherms with H3 hysteresis loops, similar to the xerogel samples, and at 1,000 °C the Type II isotherms indicate pores collapse [33]. The thermally treated sonogels, in comparison with the corresponding xerogel samples, showed larger pore sizes, larger total pore volumes and reduced surface areas. This is in good agreement with a recent report dealing with ultra-sonication effects in xerogels with high IL content [34].

3-3. Pore Size Distribution

Narrow size distributions were obtained only for the xerogel and sonogel samples, dried at 60 °C and thermally treated at 150 °C (Fig. 5). The PSD is slightly broader and the pores are larger in the sonogels. With the increase of the calcination temperature, above 500 °C, the PSD becomes broader, as a result of disruption of the walls between some pores, leading to overall pore size increase. Calcination temperatures over 500 °C are too high for obtaining materials with narrow size distribution. PSD reveals also that the pore sizes of the present materials are in the mesoporous range.
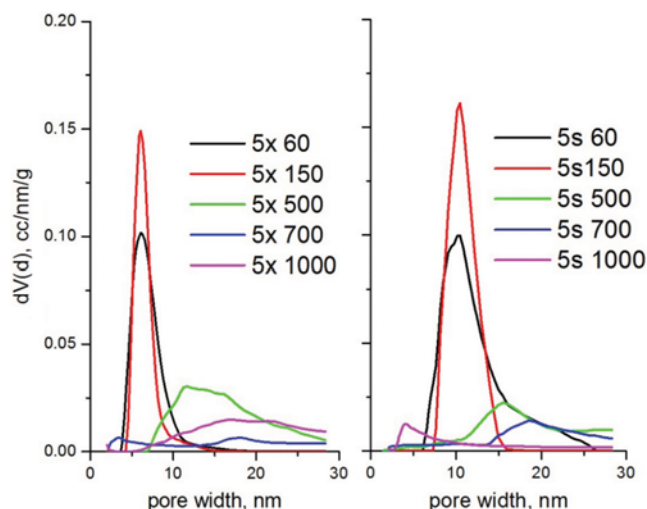

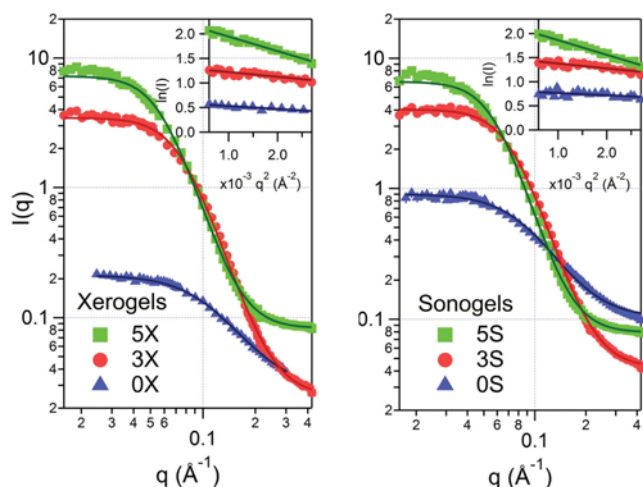Fig. 5. Pore size distributions calculated by DFT of the thermally treated samples.

Fig. 6. SANS scattering curves of xerogels (left) and sonogels (right). Continuous lines represent fitting by Eq. (1). In the Inset the Guinier fits are shown; here the data are shifted vertically for better view.

Fig. 7. Radii of gyration and correlation lengths, obtained from the SANS data.

Verma and co-workers also obtained a more uniform pore size distribution for sonogels in comparison with the xerogels [34].

4. SANS

The scattering intensity curves for xerogels and sonogels are shown in Fig. 6. They are characteristic for a material with inhomogeneities having a characteristic size, as seen by the broad plateau with decay starting at higher q values. These can be attributed to the primary particles that form in the initial phase of the condensation reaction. The simplest estimation of the particle size is the Guinier approximation, which can be used on the small q part of the data (inset in Fig. 6). Compact particles with rough, fractal-like surface can be modelled by Eq. (1):

$$I(q) = \frac{K}{(1+q^2\xi^2)^p} + bg \qquad (1)$$

where K is a scale factor related to the number density and contrast of the particles, ξ is a characteristic length related to the particle size and p is related to the surface roughness. The bg term contains the incoherent background coming mostly from the hydrogen atom content of the materials. The radius of gyration Rg and the correlation length ξ are not necessarily proportional to each other because the exponent p changes from case to case, but both can be considered as an approximate measure of the size of the scattering entity [35]. Interparticle interference effects are not included in this model, as in the given q-range there is no visible decrease or increase of the scattering intensity toward low q values. It is known that at a larger magnification, (that is, at lower q) a fractal-like assembly of the primary particles would be seen [36, 37]. Data fitting was performed by the NCNR reduction and analysis package written for the Wavemetrics Igor Pro software [38].

The scattering data show that the primary particle size in the xerogels and sonogels is about 2 nm, while at higher ionic liquid content they grow to 4-6 nm (Fig. 7). No appreciable difference could be seen between the structure of sonogels and xerogels.

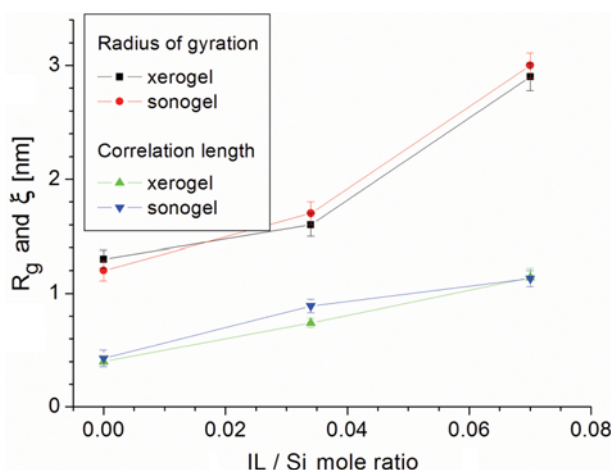In general, sonication applied during synthesis does not affect the size of monomer particles but may influence their secondary aggregation [36,37,39]. In the present materials, the SANS data did not reveal any influence of ultrasonication on the level of the primary particle formation, while the presence of ionic liquid appears to slow down the polycondensation reaction, thus leading to increase of the primary particle size.

CONCLUSIONS

Xerogels containing short chain ionic liquid, have been prepared by ultrasonication and characterized by a variety of techniques. The ionic liquid used as co-solvent played both catalytic and templating roles, as shown by the decrease of gelation time and influence on the development of different porosity. Application of ultrasound influenced the pore size distribution, surface area and pore volume. Nitrogen adsorption data show that the ultrasonic field action during the gelification leads to larger pore sizes, bigger pore volumes and smaller surface areas in the calcined materials. The pore size is almost double for sonogel samples with the highest studied IL content, compared to the non-sonicated xerogels. Increasing calcination temperatures caused a decrease of the specific surface areas due to the sintering which followed the IL elimination. The primary particle sizes do not differ significantly upon applying ultrasound, but the addition of IL slows down the polycondensation and produces larger particles.

ACKNOWLEDGEMENTS

REFERENCES

1. R. K. Donato, M. V. Migliorini, M. A. Benvegnú, M. P. Stracke, M. A. Gelesky, F. A. Pavan, C. M. L. Schrekker, E. V. Benvenutti, J.

Dupont and H. S. Schrekker, *J. Sol-Gel Sci. Technol.*, **49**, 71 (2009).

2. J. Dupont, R. F. de Souza and P. A. Z. Suarez, *Chem. Rev.*, **102**, 3667 (2002).

3. Y. Zhou, *Curr. Nanosci.*, **1**, 35 (2005).

4. A. Karout and A. C. Pierre, *J. Non-Cryst. Solids*, **353**, 2900 (2007).

5. K. S. Yoo, T. G. Lee and J. Kim, *Micropor. Mesopor. Mater.*, **84**, 211 (2005).

6. S. Dai, Y. H. Ju, H. J. Gao, J. S. Lin, S. J. Pennycook and C. E. Barnes, *Chem. Commun.*, 243 (2000).

7. L. Viau, M. Néouze, C. Biolley, S. Volland, D. Brevet, P. Gaveau, P. Dieudonné, A. Galarneau and A. Vioux, *Chem. Mater.,* **24**, 3128 (2012).

8. C. M. Wu, S. Y. Lin and H. L. Chen, *Micropor. Mesopor. Mater.*, **156**, 189 (2012).

9. A. Karout and A. C. Pierre, *Catal. Commun.*, **10**, 359 (2009).

10. M. A. Neouze, J. Le Bideau, P. Gaveau, S. Bellayer and A. Vioux, *Chem. Mater.*, **18**, 3931 (2006).

11. C. M. Wu, S. Y. Lin, K. Y. Kao and H. L. Chen, *J. Phys. Chem. C*, **118**, 17764 (2014).

12. E. Fagadar-Cosma, Z. Dudás, M. Birdeanu and L. Almásy, *Mater. Chem. Phys.*, **148**, 143 (2014).

13. D. A. Donatti and D. R. Vollet, *J. Non-Cryst. Solids*, **208**, 99 (1996).

14. E. Blanco, L. Esquivias, R. Litran, M. Piñero, M. Ramírez-del-Solar and N. de la Rosa-Fox, *Appl. Organomet. Chem.*, **13**, 399 (1999).

15. K. S. Gandhi and R. Kumar, *Sadhana*, **19**, 1055 (1994).

16. N. Enomoto, A. Kumagaia and J. Hojo, *J. Ceram. Process. Res.*, **6**, 286 (2005).

17. C. Savii, L. Almásy, C. Ionescu, N. K. Székely, C. Enache, M. Popovici, I. Sora, D. Nicoara, G. G. Savii, D. Susan-Resiga, J. Subrt and V. Štengl, *Proc. Appl. Ceram.*, **3**, 59 (2009).

18. C. M. Wu and S. Y. Lin, *Trans. Mat. Res. Soc. Jpn.*, **37**, 123 (2012).

19. L. Rosta, *Appl. Phys. A*, **74**, S52 (2002).

20. C. J. Brinker and G. W. Scherer, *Sol-Gel Science, The Physics and Chemistry of Sol-Gel Processing*, Academic Press, New York (1990).

21. R. Al-Oweini and H. El-Rassy, *J. Mol. Struct.*, **919**, 140 (2009).

22. G. Socrates, *Infrared and Raman Characteristic Group Frequencies: Tables and Charts*, John Wiley& Sons Ltd., Chichester (2001).

23. A. Duran, J. M. Fernandez-Navarro, P. Casariego and A. Joglar, *J. Non-Cryst. Solids*, **82**, 391 (1986).

24. R. F. S. Lenza and W. L. Vasconcelos, *Mater. Res.*, **4**, 175 (2001).

25. N. O. Gopal, K. V. Narasimhulu and J. L. Rao, *Spectrochim. Acta A*, **60**, 2441 (2004).

26. A. Bertoluzza, C. Fagnano, M. A. Morelli, V. Gottardi and M. Guglielmi, *J. Non-Cryst. Solids*, **48**, 117 (1982).

27. P. K. Ojha, S. K. Rath, T. K. Chongdar, N. M. Gokhale and A. R. Kulkarni, *New J. Glass Cer.*, **1**, 21 (2011).

28. D. J. Neivandt, M. L. Gee, C. P. Tripp and M. L. Hair, *Langmuir*, **13**, 2519 (1997).

29. N. E. Heimer, R. E. Del Sesto, Z. Meng, J. S. Wilkes and W. R. Carper, *J. Mol. Liq.*, **124**, 84 (2006).

30. K. S. W. Sing, D. H. Everett, R. A. W. Haul, L. Moscou, R. A. Pierotti, J. Rouquerol and T. Siemieniewska, *Pure Appl. Chem.*, **57**, 603 (1985).

31. M. Thommes, *Chem. Ing. Technol.*, **82**, 1059 (2010).

32. M. Thommes, B. Smarsly, M. Groenewolt, P. I. Ravikovitch and A. Neimark, *Langmuir*, **22**, 756 (2006).

33. S. Lowell, J. E. Shields, M. A. Thomas and M. Thommes, *Characterization of Porous Solids and Powders Surface Area, Pore Size and Density*, Springer Science+Business Media, LLC, Originally published by Kluwer Academic Publishers (2004).

34. Y. L. Verma, M. P. Singh and R. K. Singh, *J. Nanomater.*, **2012**, 570719 (2012).

35. G. Beaucage, in: *Polymer Science: A Comprehensive Reference*, Vol. 2, pp. 399-409. K. Matyjaszewski and M. Möller Eds., Elsevier BV, Amsterdam (2012).

36. N. N. Gubanova, A. Ye. Baranchikov, G. P. Kopitsa, L. Almásy, B. Angelov, A. D. Yapryntsev, L. Rosta and V. K. Ivanov, *Ultrason. Sonochem.*, **24**, 230 (2015).

37. V. K. Ivanov, G. P. Kopitsa, F. Yu. Sharikov, A. Ye. Baranchikov, A. S. Shaporev, S. V. Grigoriev and P. K. Pranzas, *Phys. Rev. B*, **81**, 174201 (2010).

38. S. R. Kline, *J. Appl. Cryst.*, **39**, 895 (2006).

39. D. R. Vollet, R. R. Torres, D. A. Donatti and A. Ibanez-Ruiz, *Phys. Stat. Sol. A*, **202**, 2700 (2005).